Journal of Materials Chemistry C

ROYAL SOCIETY OF CHEMISTRY

PAPER

View Article Online
View Journal | View Issue

Check for updates

Cite this: J. Mater. Chem. C, 2025, 13, 4055

Ultra broadband yellow emitting lead-free metal halide perovskite like compounds with near-unity emission quantum yields†

Sayed Ali Khan, *[ab] Noor Zamin Khan,[c] Jahangeer Ahmed,[d] Marcin Runowski,[f] Saad M Alshehri,[d] Simeon Agathopoulos,[e] Simon J. Teat[g] and Jing Li *[ab]

Received 12th November 2024,
Accepted 29th December 2024

DOI: 10.1039/d4tc04804k

rsc.li/materials-c

Metal halide perovskites (MHPs) are interesting semiconductor materials with potential for use in optoelectronic and photonic devices. Their practical applications are hindered due to the negative environmental effects of the lead ions (Pb^{2+}) used in these materials and stability issues. Exploring new environmentally friendly materials with lead-free metal halides and investigating the factors affecting their optical properties and stability are essential. The broadband emission and high (near-unity; ~100%) photoluminescence quantum yield (PLQY) of low-dimensional copper(I) halides make them great candidates for the next-generation luminescent materials for lighting applications. Here, a Cu(I) iodide based organic/inorganic hybrid halide (benzo-15-crown-5)$_2$NaH$_2$OCu$_4$I$_6$ (BCNCI) with a zero-dimensional (0D) cluster was prepared. The BCNCI has a broadband yellow emission peaked at 548 nm with a near-unity PLQY (99.1%) upon excitation at 365 nm (ultraviolet). Upon excitation at 450 nm (blue), a high PLQY of 82% was also achieved. The luminescence mechanism was discussed in detail. Interestingly, BCNCI exhibits ultra-broad band excitation in the 300–500 nm range, which matches commercially available UV and blue-emitting chips. Compared to commercial YAG:Ce^{3+} phosphors, the emission spectrum is sufficiently broad to cover the visible spectral region. This work illustrates a good example of developing an environmentally friendly white light source, using high-performance copper halides with adequate broadband excitation and emission.

1. Introduction

Modern lighting sources have been revolutionized by solid-state lighting (SSL) technology, which has several benefits, including low energy consumption, environmental friendliness, quick response time, high stability, and low-voltage power supply. Lighting applications benefit greatly from single materials that emit white light effectively and steadily. However, using a single material to provide photon emission that spans the full visible spectral region is challenging.[1,2] For instance, because of their simplicity of manufacture, low cost, and high efficiency, the use of blue emitting chips (GaN) with yellow emitting $Y_3Al_5O_{12}$:Ce^{3+} (YAG:Ce^{3+}) phosphors plays a notable role in the creation of commercially available white light sources.[3–6] However, the lack of the red light component in the generated white light prevents it from having the ideal color balance for good color rendering.[7–9] In light of this, identifying luminescent materials with broadband emissions spanning the entire visible region and capable of being effectively excited by blue light is currently of crucial importance. Due to their remarkable features, including adjustable emission over the visible range, good defect tolerance, and low-cost solution processing, metal halide perovskites are rising quickly improving the field of optoelectronic devices.[10–12] Low-dimensional metal halides stand out for their particular photophysical characteristics because of promising quantum confinement effects.[13,14] For example, the photoluminescence quantum yields (PLQYs) of the perovskite nanocrystals (NCs)

[a] Hoffmann Institute of Advanced Materials, Shenzhen Polytechnic University, Liuxian Blvd, Nanshan District, Shenzhen, 5018055, P. R. China. E-mail: sayedali@szu.edu.cn
[b] Department of Chemistry and Chemical Biology, Rutgers University, Piscataway, New Jersey, 08854, USA. E-mail: jingli@rugers.edu
[c] School of Physics and Material Sciences, Guangzhou University, Guangzhou, 510006, China
[d] Department of Chemistry, Collage of Science, King Saud University, Riyadh 11451, Saudi Arabia
[e] Department of Materials Science and Engineering, University of Ioannina, Ioannina GR-451 10, Greece
[f] Adam Mickiewicz University, Faculty of Chemistry, Uniwersytetu Poznańskiego 8, Poznań 61-614, Poland
[g] Advanced Light Source, Lawrence Berkeley National Laboratory, Berkeley, California, 94720, USA

† Electronic supplementary information (ESI) available. See DOI: https://doi.org/10.1039/d4tc04804k

have now reached close to unity, and the green and red electroluminescent devices have been reported to have the highest external quantum efficiencies that reach 28.1% and 25.8%, respectively.[15,16] Similarly, the effective blue light emission of perovskite-LEDs has surpassed 14.82%.[17,18] White light emission from a single emitter layer is significant for lighting applications as it simplifies device layout and prevents self-absorption and color instability in mixed and multiple emitters.[1]

Mechanisms like phosphorescence, dopant emission and emission of self-trapped excitons (STEs), which are usually found in semiconductors with localized carriers and a soft lattice, are the source of broadband warm white light emission.[1,19] According to the Hemamala mechanism, the STEs caused by the soft crystal lattice and the exciton–phonon interaction are more specifically affected by the dimensionality of the crystal structure.[2,20] More intriguingly, in low-dimensional metal halides, metal polyhedra are separated by surrounding inorganic and organic motifs, leading to robust exciton recombination with highly efficient STE emission.[21–24] Metal halide perovskites (MHPs) have received much attention as broadband emissive materials, especially those with low-dimensional crystal structures,[25,26] rarely achieving high PLQYs.[27] Instead, their reliance on lead-based compounds that are water soluble, exhibiting inferior chemical stability, and the lack of systematic knowledge of the causes of white emission are additional issues regarding their use as emitters.

The remarkable optical and optoelectronic characteristics of solar cells and LEDs, as well as their quick rise in efficiency, have drawn scientists from a wide range of fields. However, many preparation advancements to date (colloidal nanocrystals and thin films) and the most efficient devices are based on Pb-based halide perovskites, which have made commercialization of these devices problematic due to Pb's toxicity. Due to this, there has been a lot of work in the past several years in the hunt for Pb-free halide perovskites with decreased toxicity.[28–30]

The toxicity of the primary component, *i.e.* lead (Pb^{2+}), is a significant concern that restricts the commercialization of metal halide perovskite materials.[31–33] Furthermore, for practical application in lighting and displays, the stability of metal halide perovskites must be improved. Therefore, developing extremely stable, broad band-emitting metal halide compounds made of eco-friendly (lead-free) metals is urgently required.[34,35] Recently, researchers have been increasingly choosing to produce Cu(I)-based metal halides due to their great abundance, low cost, highly efficient tunable emission, and nontoxicity.[36–39] More interestingly, copper-based metal halides can easily build low-dimensional structures with superior PLQYs and excellent stability, because of their small ionic radii and stable metal oxidation state. In addition, recently there have been multiple reports of low-dimensional copper-based halides with superior PLQYs. For example, T. Jun and co-workers first synthesized $Cs_3Cu_2I_5$, all-inorganic compounds with an isolated 0D structure, exhibiting blue emission, peaking at 445 nm with very high PLQYs of 90% for single crystals and 60% for films, respectively.[40] This demonstration revolutionizes the development of novel solution-processable lead-free metal halides. However, the excitation wavelength of this and other reported Cu(I) based all-inorganic metal halides located in the range of 200–350 nm with a maximum peak position of 290 to 300 nm.[41,42] The photoluminescence excitation spectrum in this wavelength range, *i.e.*, the deep ultraviolet range, significantly restricts their further commercial applications.

A fascinating class of functional materials known as organic–inorganic hybrid metal halides also offers a surprising range of structural variations and an enormous array of potential applications.[43–46] In contrast to inorganic solids, organic–inorganic hybrid metal halides enable us to construct an inorganic lattice selectively.[47–49] For instance, S. Li *et al.* developed a lead-free Cu(I) based organic–inorganic perovskite type $[(12\text{-crown-4})_2K]_2[Cu_4I_6]$ compound, which emits a broadband of the greenish-yellow emission band peaking at 545 nm with a PLQY of 97%.[50] Similarly, most recently, H. Huang *et al.*[51] reported another crown-ether-based compound with a composition of $(18\text{-crown-6})_2Na_2(H_2O)_3Cu_4I_6$ having a zero-dimensional (0D) cluster of Cu(I) based halides (organometallic). The discovered compounds have a high PLQY of 91.8% and generate a brilliant, broad-spectrum green emission with a peak at 535 nm. More intriguingly, the broadband excitation of both new crown-ether-based compounds is a perfect match for the widely used blue-emitting chip. However, the emission band is not broad enough to cover the complete visible spectrum for creating single-phase white LEDs. Additionally, the synthesis was conducted using a harmful and combustible organic solvent like acetone. We synthesized single-phase materials with many types of luminescence in our prior work, which is important in many sectors since they exhibit a simultaneous optical response to a variety of stimuli.[52–54]

Although the aqueous synthesis processes have gained increasing attention due to the need for sustainable development, their use in synthesizing luminous Cu(I) hybrid materials has not been extensively explored. In this work, a novel Cu(I) based organic/inorganic metal halide is synthesized in water using benzo-15-crown-5 ether as the organic component to achieve the single-phase white lighting emitting material by a green reaction route. More specifically, the compound $(\text{benzo-15-crown-5})_2NaH_2OCu_4I_6$ with a 0D structure is designed when benzo-15-crown-5 ether (crown-ether) couples with sodium ions (Na^+) to generate complex cations, which are then combined with an anionic Cu_4I_6 cluster. According to the calculations using density functional theory (DFT), the majority of the electronic states in 0D $[(\text{benzo-15-crown-5})_2NaH_2O][Cu_4I_6]$ are contributed by the 0D clusters made up of tetrahedral copper halides. At the same time, the organic portion only forms a 0D cluster with isolated $[Cu_4I_6]^{-2}$ anions in the 2D direction. The extent of exciton delocalization significantly influences the rate of radiative recombination.[55,56] As a result, under 365 nm (UV) and 450 nm (blue) light excitation, respectively, the $[(\text{benzo-15-crown-5})_2NaH_2O][Cu_4I_6]$ single crystal exhibits high PLQYs of 99.1% and 82%. The sample exhibits a substantial Stokes shift of 100 nm at an ambient temperature with an FWHM of 180 nm. Meanwhile, the $[(\text{benzo-15-crown-5})_2NaH_2O][Cu_4I_6]$ excitation shows dual-peak spectra peaking at 365 and 450 nm, which is well compatible with the emission of commercially available ultraviolet (UV) and blue LED chips. Additionally, the emission

spectrum is broader than the yellow emission spectrum of commercial YAG:Ce^{3+} phosphors and covers the entire visible range (480–800 nm). The current work serves as a good example in the design and development of low-dimensional, ultra-broadband emitting metal halide materials for potential applications in single-phase white light emitting devices.

2. Materials and methods

Materials

Benzo-15-crown-5 ($C_{14}H_{20}O_5$) with 98% purity, acetone (C_3H_6O, 99.5%), sodium iodide (NaI), and hypophosphorous acid (H_3PO_2, 50% in water by weight) were all acquired with VWR, while copper iodide (CuI) with 98% purity was obtained from Alfa Aesar. All the materials were used directly without any other further verification and treatments.

Synthesis

Sodium iodide (NaI), copper(I) iodide (CuI), and benzo-15-crown-5 ($C_{14}H_{20}O_5$) with 2 mmol each were dissolved in 2 mL of deionized water at 80 °C with continuous stirring. H_3PO_2 (0.5 mL) was added to the solution to maintain the Cu(I) state in the solution. After stirring for 24 hours at 80 °C, a suspension was observed in the solution which was filtered and dried at room temperature. Polycrystalline materials with yellow color under ordinary daylight and more bright crystals under 365 nm UV light were obtained which were further sintered at 80 °C under vacuum. To produce the [(benzo-15-crown-5)$_2$NaH$_2$O][Cu_4I_6] single crystal for single crystal XRD and phase analysis, benzo-15-crown-5 (2 mmol), CuI (2 mmol), NaI (2 mmol), and H_3PO_2 (2.5 mL) were first mixed in 10 mL of acetone at 80 °C while stirring to create a transparent solution. The solution was filtered, and the solvent was then gradually evaporated at room temperature over numerous days to produce large-sized crystals.

Characterization

Single crystal X-ray diffraction (SCXRD) data for the synthesized 0D-[(benzo-15-crown-5)$_2$NaH$_2$O][Cu_4I_6] samples were obtained at 250 K on a Bruker D8 venture diffractometer with Cu Kα radiation or at 173 K on a Bruker D8 VENTURE Metal jet PHOTON II diffractometer with gallium micro-focus metal jet X-ray sources with λ = 1.34139 Å. Similarly, the powder X-ray diffraction of the powder samples was measured at different times for phase analysis and stability. The powder samples were subjected to powder X-ray diffraction (PXRD) analysis using a Rigaku Ultima-IV diffractometer with Cu Kα radiation (λ = 1.5406 Å). The data were gathered in the 2θ range of 3–40° at room temperature with a scan speed of 0.5° min^{-1} and an operating power of 40 kV/40 mA.

The energy dispersive X-ray spectroscopy (EDS) data with elemental color mapping were acquired on an Oxform-XmaX80 detector coupled to the FE-SEM while scanning electron microscopy (SEM) images of the produced 0D-[(benzo-15-crown-5)$_2$NaH$_2$O][Cu_4I_6] crystals were done on a Zeiss-Sigma FE-SEM. A 5 kV working voltage was used to acquire elemental color mapping. The room-temperature solid-state photoluminescence excitation (PLE) and emission (PL) were recorded on a Horiba Duetta fluorescence spectrometer. More specifically, the powder sample of 0D-[(benzo-15-crown-5)$_2$NaH$_2$O][Cu_4I_6] hybrid materials were evenly dispersed and sandwiched among the two glass slides for the recording of the room temperature PLE and PL. Solid-state UV-vis spectroscopy was performed on a Shimadzu UV-3600 spectrometer using powder materials. The photoluminescence quantum yields (PLQYs) of the powder materials were measured using commercial sodium salicylate (for 365 nm PLE) and YAG:Ce^{3+} (for 450 nm PLE) as references and Hamamatsu S3 Photonics C9920-03 absolute quantum yield equipment with a 150 W xenon monochromatic light source. To measure the stability of the synthesized powder against temperature, the powder sample was heated from room temperature (RT) to 600 °C at an increasing rate of 10 °C min^{-1} for thermogravimetric (TGA) analysis using a TGA 550 (TA Instruments) analyzer.

The temperature-dependent photoluminescence spectra (PL) and time-resolved PL decay time profiles of the synthesized powder sample of the hybrid materials were assessed using homemade time-correlated single photon counting apparatus. This device used a Janis cryostat model V500, a single photon counting avalanche photodiode (PMD 50, Picoquant, 45 ps response time), a time spectrometer, and 380 nm pulsed light from a frequency-doubled femtosecond solid-state laser (Maitai-Spectra Physics, 100 fs pulse, 10 kHz repetition rate). More specifically, a 10 mm diameter die was used to press the 0D-[(benzo-15-crown-5)$_2$NaH$_2$O][Cu_4I_6] powder into a pellet shape at a pressure of about 2000 psi. A 500 mm biconvex lens was used to detect the photoluminescence signal produced by the sample's radiation. A 50/50 non-polarizing beam splitter cube was used to divide it between the photodiode and the PL fiber spectrometer. At a 532 nm long pass filter, the photoluminescence signals were obtained using an average power of 0.55 mW, and decays were recorded with at least 1000 channels (Semrock). The photoluminescence decays were individually fitted using a bi-exponential fitting with lifetime contributions estimated as averaged amplitudes.

DFT calculation

All the calculations were performed *via* the DFT method using the Vienna ab initio simulation package (VASP).[57] To explain electron–ion interactions, the projected-augmented wave (PAW) method was used.[58,59] The generalized gradient approximation (GGA) with the Perdew–Burke–Ernzerhof (PBE) functional was used for all the calculations.[60] For the optimized structure, the total energy was converged to an accuracy of 1×10^{-7} eV. The energy cutoff used in the calculation was 520 eV. The Brillouin zone was obtained using a 2 × 2 × 1 Monkhort–Pack *k*-point grid. The DFT-D3 method is used for the account of van der Waals correction.[61] All the atoms were allowed to relax during the structure optimization until the forces were less than 0.001 eV Å^{-1}.

3. Results and discussion

The yellow crystals were formed using an aqueous synthesis technique. Briefly, benzo-15-crown-5 ether, NaI, and CuI were

dissolved in 2 mL of deionized water and agitated at 75 °C. The solution was then supplemented with 0.5 mL of H_3PO_2 that contained 50% water. 24 hours of continuous stirring resulted in a suspension, which led to the formation of the target crystals after filtering and washing. The experimental section contains a detailed explanation of the synthesis process. The crystal structure of the as-grown crystals was determined using the single crystal X-ray diffraction (SCXRD) technique, and it is identified as $(C_{14}H_{20}O_5)_2NaH_2OCu_4I_6$ with the lattice parameters a = 10.9241 Å, b = 15.7438 Å, and c = 21.772 Å, β = 91.120 (1)° and V = 3743.80 (15) Å^3. The corresponding crystallographic information file (CIF) for the synthesized $(C_{14}H_{20}O_5)_2NaH_2OCu_4I_6$ perovskite type compound is included in the ESI,† and Table 1 lists the key crystallographic data and analysis parameters.

The benzo-15-crown-5 ether readily coordinates with the alkali metal or alkaline rare-earth metal in the crystallographic structure of $(C_{14}H_{20}O_5)_2NaH_2OCu_4I_6$, and the two benzo-15-crown-5 ether complexes are attached to one Na^+ ion by a H_2O molecule as shown in Fig. 1a. The typical synthon for the ionic constituent copper(I) halides in organic–inorganic hybrid compounds was a rhombohedron with copper (Cu^+) and halide (Cl^-, Br^- and I^-) atoms at alternate corners, which may be fused or linked by edges or sharing corners to produce aggregates with superior clarity.[51,62] In order to coordinate the Cu^+ ions, three I^- ions assemble to create a CuI_3 complex. A $(Cu_4I_6)^{2-}$ cluster is formed by these complexes, which are joined to one another by edges and nodes and are distributed throughout eight places (Fig. 1b). Table S1 in the ESI† provides a detailed illustration of the bond lengths in the crystallographic structure of $(C_{14}H_{20}O_5)_2NaH_2OCu_4I_6$. The 3D representation of the crystal structure of the synthesized compound (benzo-15-crown-5)$_2NaH_2OCu_4I_6$ is shown in Fig. 1c, projected along the a-axis, to illustrate the 0D framework with isolated $(Cu_4I_6)^{2-}$ constituents.

The phase purity of the synthesized (benzo-15-crown-5)$_2$-$NaH_2OCu_4I_6$ 0D cluster was thoroughly investigated, and structural formation and elemental composition were carefully measured. Fig. 2a shows the powder XRD profile of the synthesized (benzo-15-crown-5)$_2NaH_2OCu_4I_6$ compound, which matches well with the simulated pattern generated by the single crystal structure data, confirming good phase purity. The synthesized sample was further sintered at 75 °C under vacuum for 12 hours. The (benzo-15-crown-5)$_2NaH_2OCu_4I_6$ powder sample has particles with a diameter of approximately micrometer (μm) size, according to the scanning electron microscopy (SEM) image (Fig. 2b). The absence of the impurity phase is also seen from the homogenous distributions of the copper (Cu) and iodine(I) elements in the (benzo-15-crown-5)$_2NaH_2OCu_4I_6$ crystallites, as confirmed by the elemental mapping obtained by energy dispersive X-ray spectroscopy (EDS), which is shown in Fig. 2c–e. One effective method for visualizing the atomic-level structure of organic–inorganic hybrid perovskite (OIHP) materials is transmission electron microscopy (TEM), which offers crucial and important directions for high-performance OIHP-related devices. Nevertheless, the low electron beam stability of these organic–inorganic hybrid compounds significantly restricts their usefulness in TEM. The synthesized BCNCI sample's morphology was subsequently investigated using TEM and HTEM, which verified that stable BCNCI particles with a micron size could be easily identified (Fig. 2f and g). Thermal stability is a crucial factor in determining whether the produced luminescence material is suitable for applications in white LEDs. The thermogravimetric analysis (TGA) curve depicted in Fig. 2i shows that the thermal degradation of the synthesized (benzo-15-crown-5)$_2NaH_2OCu_4I_6$ compound is a multistage process. The first stage demonstrates that the degradation temperature (TD) is around 180 °C, demonstrating that the as-prepared compound is stable to at least ≈180 °C. The variance in the first step is attributed to the degradation of the Na-coordinated benzo-15-crown-5; 40% of the weight loss was observed in this stage, reaching a temperature of 350 °C. The weight loss in the second stage is related to the degradation of Cu_4I_6, which leads to the remaining weight loss until 700 °C. The mass of the legends was further confirmed by high resolution mass spectrometry (Fig. S1, ESI†) which further confirms the stability of the synthesized compound for the potential use in single-phase white-LEDs.

The crystals synthesized *via* a simple aqueous solution route exhibit strong yellow emissions when exposed to UV/blue light (inset of Fig. 3a). Fig. 3a shows the photoluminescence emission (PL) and excitation (PLE) spectra of the (benzo-15-crown-5)$_2$-$NaH_2OCu_4I_6$ powder sample at room temperature. The PLE has a broad band between 200 and 500 nm, centered on 400 nm, which is compatible with commercially available UV (365 nm) and blue (450 nm) emitting chips. The room temperature (RT) PL spectrum of the synthesized sample exhibits a single and broad yellow emission band, peaking at 548 nm under excitation at around 365 nm and 450 nm. The emission spectrum of the sample has a peak at 548 nm with a full width at half-maximum of 175 nm at room temperature. Both excitation wavelengths result in a similar single band emission of the same shape, with varying intensities. The intensities were also observed identical (Fig. S2, ESI†). The broadband yellow emission covers almost the entire visible spectral region. The observed broadband yellow emission was compared with commercially available yellow emitting YAG:Ce^{3+} phosphors. More specifically, the commercially available white light source for general illumination usually uses all-inorganic $Y_3Al_5O_{12}$:Ce^{3+}

Table 1 BCNIC single crystals' basic crystal structure parameters

Chemical formula	$C_{42}H_{28}Cu_4I_6NaO_{11}$
Abbreviation	BCNCI
Molecular weight	1593.23
Temperature (K)	200
Crystal system	Monoclinic
Space group & cell formula unit	$P1\ 21/c1$ (14)
a	10.9241 Å
b	15.7438 Å
c	21.772 Å
α	90°
β	91.120 (1)°
γ	
V	3743.80 (15) Å^3

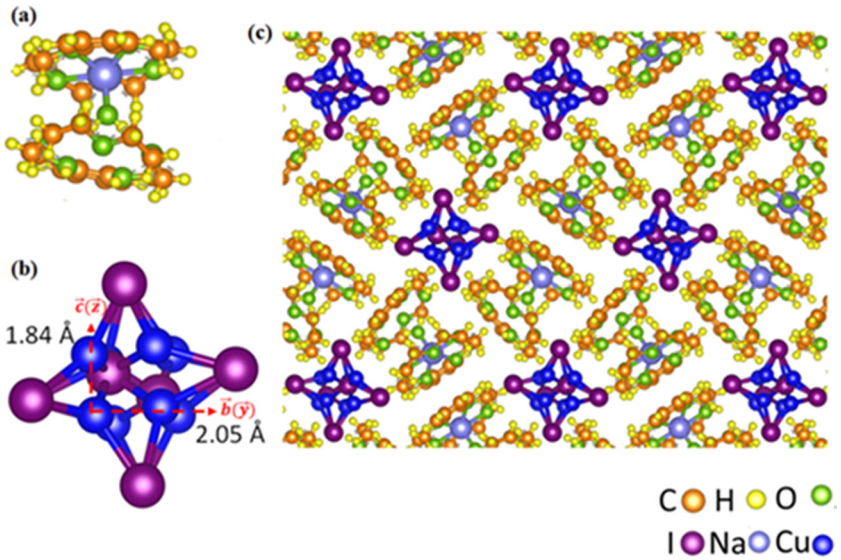

Fig. 1 (a) A detailed representation of the $[\text{benzo-15-crown-5})_2NaH_2O]^+$ cation with various orientations. Two benzo-15-crown-5 ligands and one unit of water (H_2O) molecule connected each Na ion. The H_2O molecule bridge connecting the benzo-15-crown-5 coordinated Na to another benzo-15-crown-5 molecule to generate a cationic unit, (b) a detailed view of the anionic $(Cu_4I_6)^{2-}$ polyhedral blocks. The eight sites in the structure where the four Cu^+ ions are disordered mean that they only have a 50% chance of occupying crystallographic sites. (c) The crystal structure of $\text{(benzo-15-crown-5})_2NaH_2OCu_4I_6$ along the *a*-axis reveals the 0D cluster with isolated $(Cu_4I_6)^{2-}$.

(YAG:Ce^{3+}) yellow emitting phosphors. Fig. 3b, which compares the emission spectra, indicates that the currently synthesized $\text{(benzo-15-crown-5})_2NaH_2OCu_4I_6$ compound exhibits ultra-broadband emission with a strong potential for use in single-component white-LEDs. More interestingly, the emission spectrum of the $\text{(benzo-15-crown-5})_2NaH_2OCu_4I_6$ material not only covers the red spectral region but also the cyan part which is lacking by the commercially available YAG:Ce^{3+} phosphors. Both the cyan and red spectral region gaps are critical to enhancing the quality of white light for general illumination purposes.[63–67] Fig. 3c shows the normalized PL spectra, recorded with various excitation wavelengths (365–455 nm; with a 20 nm interval). The

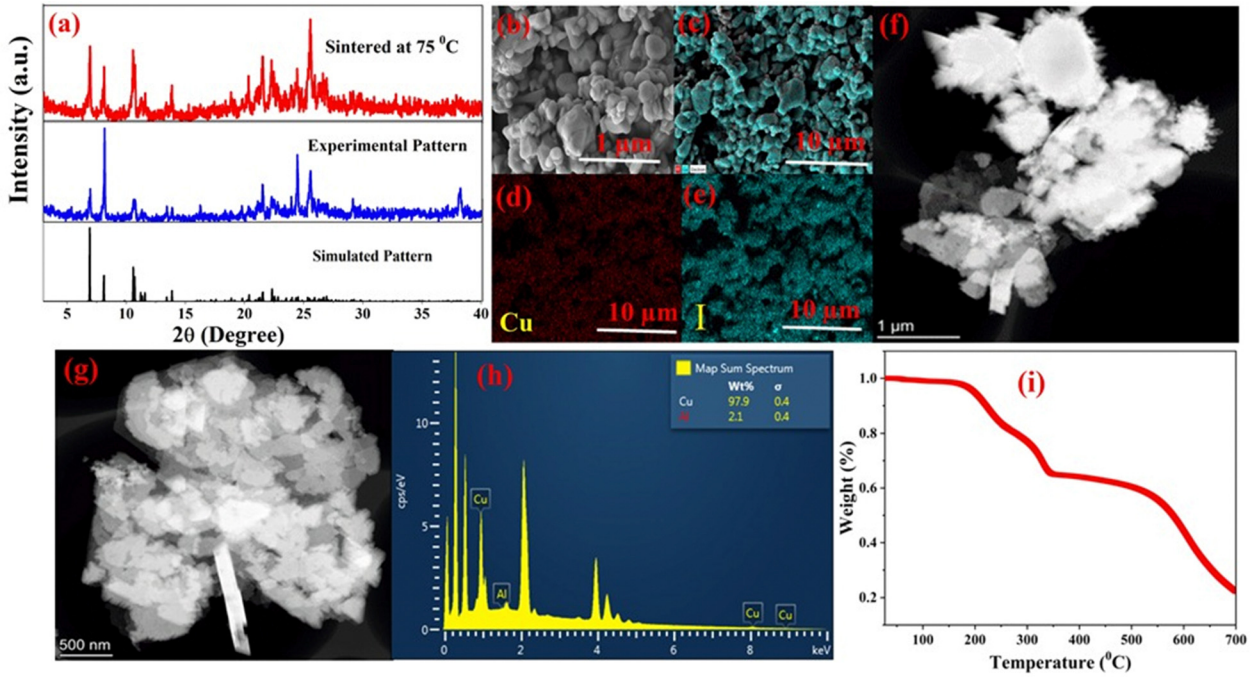

Fig. 2 Structural and elemental analyses, (a) powder X-ray diffraction pattern of the as-synthesized $\text{(benzo-15-crown-5})_2NaH_2OCu_4I_6$ compound and the compound sintered at 75 °C for 12 hours, (b) SEM image of the as-synthesized sample, (c)–(e) elemental color mapping of Cu and I elements, and (f) and (g) TEM images at various scales, (h) energy dispersive spectroscopy (EDS) plot, and (i) TGA plot of the as-synthesized $\text{(benzo-15-crown-5})_2NaH_2OCu_4I_6$ sample.

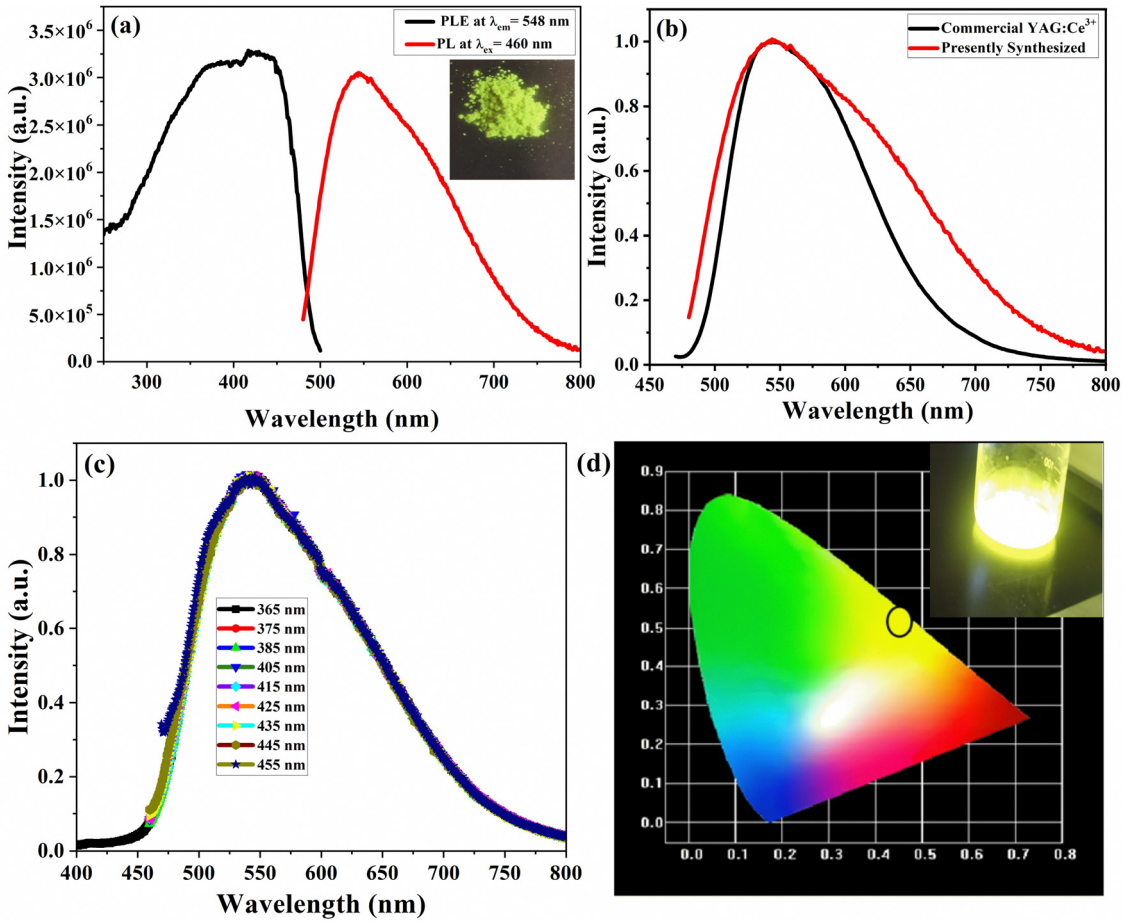

Fig. 3 Luminescence characteristics of the synthesized (benzo-15-crown-5)$_2$NaH$_2$OCu$_4$I$_6$ composition, (a) PLE and PL of the synthesized sample, the inset is a digital photograph of the crystals under 365 nm UV light, (b) comparison of the emission spectrum of the synthesized (benzo-15-crown-5)$_2$-NaH$_2$OCu$_4$I$_6$ composition with the emission spectrum of the commercially available YAG:Ce^{3+} phosphors under the same excitation, and (c) emission spectrum under various excitations from 365 nm to 450 nm, and (d) CRI color coordinate diagram with a digital photograph under UV light.

results obtained show that the emission spectrum shape is independent of the excitation wavelength. The CIE color coordinate diagram obtained from the emission spectrum is shown in Fig. 3d, which confirms the bright yellow emission color of the synthesized BCNCI compound under 365 and 450 nm PLE. The emission spectra used to calculate the PLQYs are given in the ESI† (Fig. S3a and b, ESI†). Under 365 nm and 450 nm excitation, the PLQYs are determined to be near-unity (99.2%) and 82%, respectively. These values are competed with the best PLQYs of the single-phase lead-free halides that emit a broad-band yellow light.[47–51] The (benzo-15-crown-5)$_2$NaH$_2$OCu$_4$I$_6$ material offers great advantages in safety and efficiency when compared to other halide perovskite materials.

Fig. 4a displays the absorption spectra of the BCNCI compound, which exhibits ultra-broad band absorption. According to the diffuse reflection spectra, it was observed that the measured band gap of the BCNCI powder sample is 2.95 eV. The determined band gap of the synthesized BCNCI is similar to other previously reported Cu(I)-based organometallic halides.[68–70] More specifically, the currently produced BCNCI compound's band gap is comparable to that of the 1D potassium (K) coordinated crown ether-based organometallic copper iodides ([K(C$_8$H$_{16}$O$_4$)$_2$]$_2$[Cu$_4$I$_6$]).[50] However, the band gap, 2.95 eV, is greater than the band gap, 2.43 eV, of a similar (18-crown-6)$_2$Na$_2$(H$_2$O)$_3$Cu$_4$I$_6$ (CNCI) organometallic compound with a 0D structure. It has been reported that in the recently discovered (18-crown-6)$_2$Na$_2$(H$_2$O)$_3$Cu$_4$I$_6$ (CNCI) compound, hydrogen bonds are used to bind the H$_2$O molecules and organic cations.[51] The orbitals become more or less hybridized due to the hydrogen bonding, which lowers the CNCI compound's valence band maximum (VBM) energy level and narrows the band gap. However, no hydrogen bonding was observed in the present case (BCNCI). As a result, a larger bandgap was seen for the compound BCNCI.

The structure of the BCNCI compound was optimized and relaxed to make a computational analysis. The partial density of states (PDOS) was calculated following the optimization. There are orbital populations present, according to PDOS analysis. The orbital population indicates Cu(d) strong reactivity, which is close to the Fermi level (Fig. 4b). The PDOS calculation shows the band gap between the valence band and conduction band; the estimated value for this is in the range of 2.4 eV, which is lower than the observed value (2.95 eV). More specifically, the predicted band gaps have smaller values but follow the same

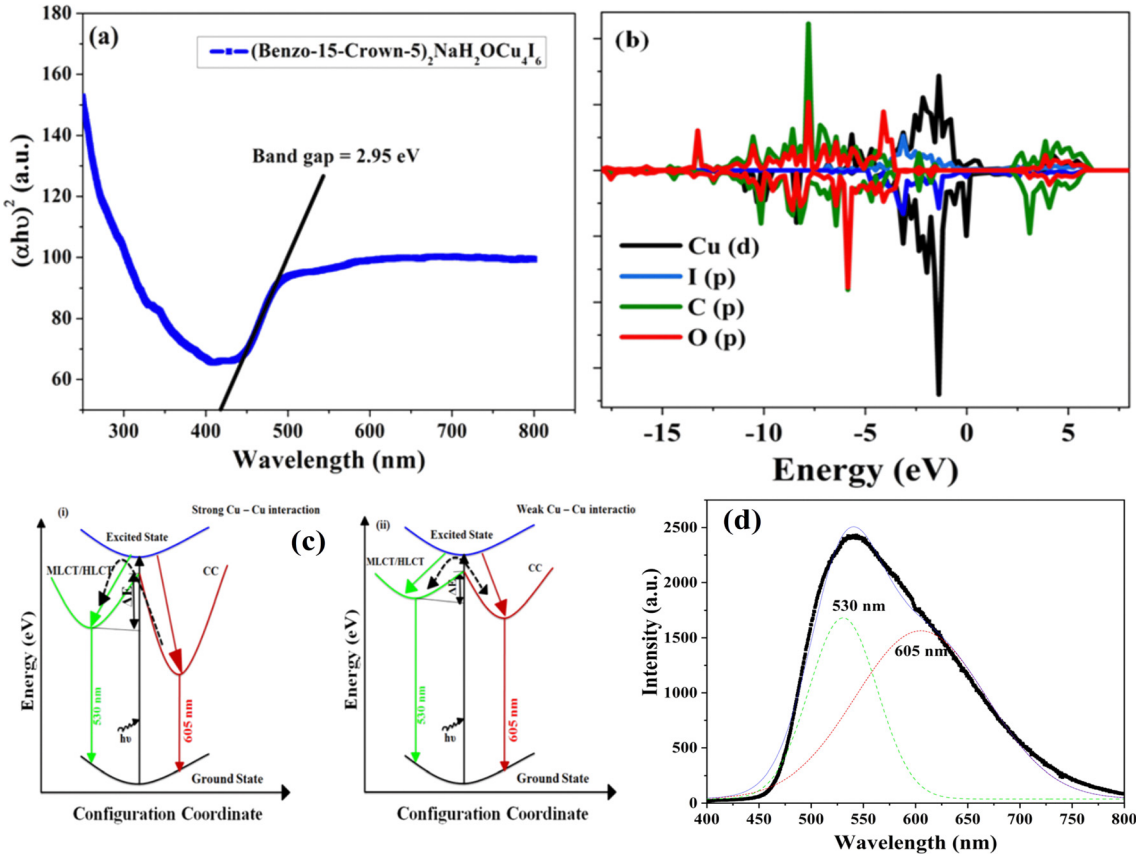

Fig. 4 Characteristics of optical bandgap calculation of the presently synthesized (benzo-15-crown-5)$_2$NaH$_2$OCu$_4$I$_6$ (BCNCI) composition: (a) diffuse reflection spectrum, (b) the partial density of states of the selected atoms, (c) schematic illustration of energy level diagram and energy mechanism, and (d) PL spectrum with deconvolution of the Gaussian fitting.

pattern as the observed optical band gaps calculated from optical absorption spectra. This is due to the fact that the generalized gradient approximation (GGA) and the local density approximation (LDA) functional alone usually underestimate the bandgaps.[21] Additionally, a study of the projected DOS (PDOS) indicates that the inorganic components—specifically, the Cu(d) and I(p) orbitals—are the main causes of the valence band maximum (VBM). The conduction band minimum (CBM) contributions, however, come from both inorganic (Cu(d) and I(p)) and organic (C(p) and O(p) atomic states of the motifs. This exhibits that the emission might be attributed to different mechanisms, namely (i) halide to ligand charge transfer (HLCT)/metal-to-ligand charge transfer (MLCT) based emission, or (M+X)LCT, which are usually seen in the compounds with long Cu–Cu distances or in other words with weak Cu–Cu interactions; or (ii) the cluster-centered (CC) transition based emission, which has been seen in numerous copper iodide-based organic–inorganic hybrid compounds with short Cu–Cu distances, such as those constructed on cubane Cu_4I_4 clusters.[71] The outcome could be single or many radiative decay routes, depending on whether one or both processes predominate.

More interestingly, according to earlier research, the photoluminescence emission of Cu(I) based organometallics, such as cubane $Cu_4I_4L_4$ (L = pyridine and phosphine), results from numerous remarkable emissive states. Extensive research over the past several decades has shown that both pathways, CC (low energy emission peak) and (M+X)LCT (high-energy emission peak), can occur at the same time.[62] However, the energy barrier between the electronic configurations is a key factor in the so-called dual emissions.[72] In more detail, the luminescence mechanism shows that the high energy band is due to an MLCT/HLCT excited state. In contrast, the low-energy band (component) of the emission spectrum corresponds to the CC excited state, which can be seen in the case of metal center contacts. The schematic illustration shown in Fig. 4c presents the luminescence mechanism of dual color emission which can be seen as a result of the synergistic interaction of two energy states, with the MLCT/HLCT excited state leading the high-energy (lower wavelength) emission band and the CC excited state leading the low-energy (higher wavelength) emission band. A series of PL measurements at various temperatures can be used to track the impact of temperature. Cu–Cu distances, as a measure of Cu–Cu interaction, are crucial for CC transition. The compounds that have Cu–Cu distances around 2.05 Å or less (as little as 2.5 Å) typically exhibit strong CC transitions.

The emission spectrum of the BCNCI compound can be de-convoluted into two Gaussian components with peaks at 530 nm and 605 nm (Fig. 4d), confirming the presence of two different types of luminescence centers in the BCNCI compound. Its broadband emission suggests that the excited states are charge transfer-type. Interestingly, its emission color can be

smoothly adjusted from 530 to 605 nm. More specifically, the observed highly efficient dual color emission is attributed to strong Cu–Cu interactions (Fig. 4d).

The temperature-dependent PL and decay time curves were thoroughly examined to better comprehend the luminescence mechanism of the synthesized BCNCI compound. The temperature decreased from 300 to 80 K, in steps of 50 K. When the temperature reached a stable point in each step, PL spectra were recorded using excitation wavelengths of 365 and 450 nm, respectively. Fig. 5a displays the emission spectra of BCNCI under 365 nm excitation at various temperatures (300–80 K), demonstrating that the emission peak positions of the PL spectrum are unaltered. Interestingly, the dual emission peaks become more prominent when the temperature decreases (a clear splitting of the band components is observed). Moreover, the full width at half maximum (FWHM) decreases with decreasing temperature. Both the lower energy (LE) and higher energy (HE) bands become more intense and narrower (decrease of FWHM) when the temperature is gradually lowered to 80 K. More precisely, the intensity of a higher energy peak increases more prominently. However, the spectral position of this peak is almost the same. In contrast, the LE peak is red shifted by around 20 nm.

The observed enhancement of the intensity of the emission spectrum with a decrease in temperature is attributed to the suppression of non-radiative recombination. More specifically, this phenomenon could be explained by decreased structural torsion and greater localization of the excited state on the molecular structure, as well as relaxed electron–phonon interactions, which boost the luminescence efficiency.[73–75] Similarly, when the temperature drops, a similar tendency of the emergence of dual peak emission spectra was also seen at 450 nm excitation as illustrated in Fig. S4 (ESI†) (the normalized temperature-dependent PL spectra under 450 nm excitation). The identical dual peak emission was observed at both the excitation of 365 nm and 450 nm. However, as the temperature decreases from 300 K to 80 K, the intensity of the emission spectrum as a result of 450 nm excitation decreases. This may be because both the processes at a given excitation (450 nm) cannot have a large population at low temperatures, due to the weak coupling and high barrier between the two electronic configurations.[72,76–80] However, increased excitation energy will increase the relative intensity of (M+X)LCT-based emission at a given temperature because more electrons are populated in the excited state.[44]

It is important to note that at 80 K, the PL spectra are divided into two distinct emission peaks at 530 and 625 nm. The observed data clearly shows the separation of the excitation and emission peaks, demonstrating the existence of two distinct luminescence centers. We believe that it is more reasonable to attribute the higher energy (lower wavelength) emission to MLCT/HLCT because it is difficult to accurately distinguish between halide-to-legend charge transfer (HLCT) and metal-to-legend charge transfer (MLCT), according to existing reports and models.[51,81–83] While the lower energy (higher wavelength)

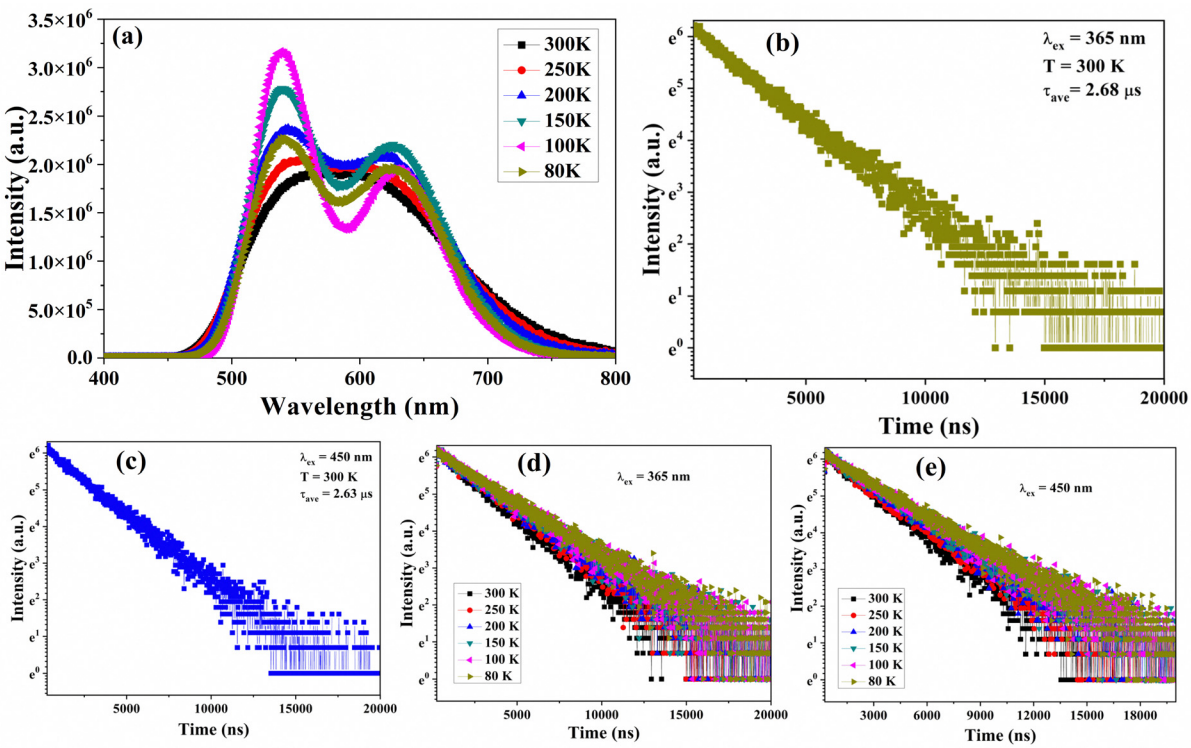

Fig. 5 Photoluminescence spectroscopic data of a BCNCI powder sample, (a) temperature dependent PL under 365 nm excitation, (b) and (c) room temperature decay time profile under 365 nm excitation, 530 nm monitored emission wavelength and 450 nm PLE, and 625 nm monitored emission wavelength, and (d) and (e) temperature dependent decay time profile λ_{ex} = 365 nm, λ_{em} = 530 nm and λ_{ex} = 450 nm, λ_{em} = 625 nm.

peak positioned at 625 nm is attributed to CC transition. More specifically, the Cu–Cu distance in BCNCI is 2.75 Å, comparable to the Cu–Cu distance in the reported MLCT or HLCT and CC transition.[84]

To have a closer look, the room temperature photoluminescence decay profile of the synthesized BCNCI compound was measured at the monitored wavelengths of 548 nm for emission and 365 or 450 nm for excitation, respectively. Fig. 5b and c show the recorded decay curves, which can be well fitted to the second-order exponential equation given below:[6,31,85,86]

$$I(t) = A_1 \exp\left(\frac{-t}{\tau_1}\right) + A_2 \exp\left(\frac{-t}{\tau_2}\right), \quad (1)$$

where I denotes the luminescence intensity, A_1 and A_2 are amplitudes, t represents the time, and τ_1 and τ_2 are the decay time components (fast and slow ones), respectively. Eqn (2) can be used for determination of the average excited state lifetime (τ^*).

$$\frac{A_1\tau_1^2 + A_2\tau_2^2}{A_1\tau_1 + A_2\tau_2} \quad (2)$$

The τ^* values for the synthesized BCNCI were found to be 2.68 and 2.63 μs, under 365 nm (UV) and 450 nm (blue) light irradiation, respectively.

Additionally, the temperature-dependent PL decay curves of the BCNCI phosphor were measured under 365 nm and 450 nm excitation. The obtained results are plotted in Fig. 5d and e, illustrating that the decay times prolonged with the temperature decreasing from 300 K to 80 K. The apparent increase in the decay time values was in the ranges of 2.68–3.52 μs and 2.63–3.47 μs, under 365 nm and 450 nm excitations, respectively. This could be related to inhibiting the thermally triggered non-radiative recombination channels and relaxed electron–phonon coupling. Interestingly, the determined decay times differed for 365 nm and 450 nm excitations, for both room temperature (RT) and low temperature (LT) regimes. The observed difference in the PL decay profiles and the corresponding lifetimes supports the existence of two different luminescence centers, which were also observed in the case of low-temperature PL.

For the practical uses of solid state lighting, the stability against moisture, light and temperature are essential issues for metal halides.[87–91] More specifically, the performance of the practical device might be significantly influenced by moisture, as the structure of the metal halide perovskites is often unstable under contact with water molecules.[49,92–95] The powder XRD (PXRD) patterns and PL spectra of the synthesized BCNCI crystals after being submerged in water for five days and stored in the open air for six months are shown in Fig. 6a and b. The PXRD patterns that depict the phase of the synthesized materials are unaltered, similar to the photoluminescence spectrum which shows essentially no alterations. Fig. 6c displays digital photographs of the BCNCI crystals immersed in

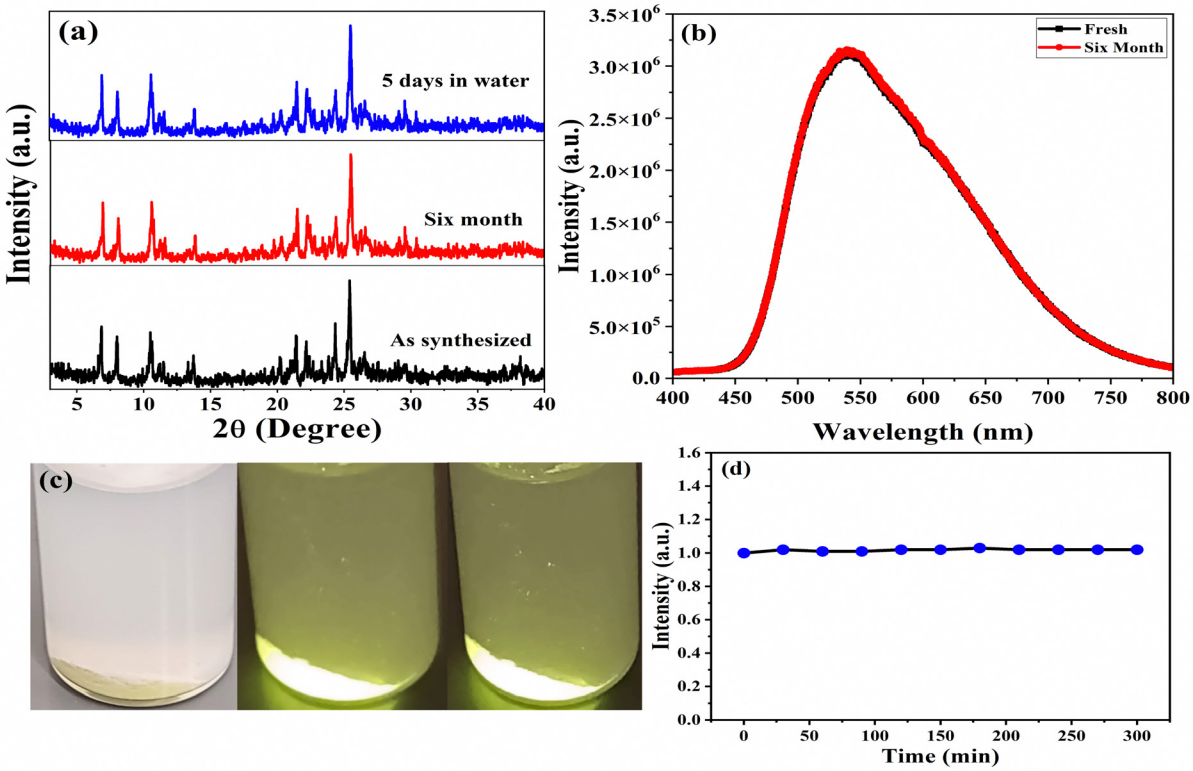

Fig. 6 Stability of the compound with time, (a) comparison of the PXRD pattern of the sample after six months and the sample dispersed in water for six months with PXRD of the fresh sample, (b) comparison of the PL spectrum of the powder sample after six months with PL of the fresh sample, (c) photographs of the fresh sample and sample dispersed in water for six days, and (d) PL intensity of the powder sample irradiated at 365 nm for 300 minutes.

water under daylight and 365 nm (UV) light irradiation. The remarkable water resistance and stability are confirmed by the detected bright yellow light, with the same photoluminescence performance as that at the initial stage. Additionally, BCNCI crystals exhibit very good photo-stability, as their integrated photoluminescence intensity nearly holds steady under continuous 300-minute exposure to 365 nm UV light.

4. Conclusions

In summary, we applied a facile aqueous synthesis route to develop unique 0D cuprous iodide hybrid (benzo-15-crown-5)$_2$NaH$_2$OCu$_4$I$_6$ crystals by combining copper iodide (CuI), sodium iodide (NaI), and benzo-15-crown-5 ether in 2 mL of deionized water at 80 °C. To maintain the Cu(I) state, a small amount of hypophosphorous acid (H_3PO_2, 50% in water by weight) was added. The cationic motif of the crystal structure of the $(C_{14}H_{20}O_5)_2NaH_2OCu_4I_6$ complex is based on the Na^+-coordinated with two crown ether molecules. The two crown ether complexes are connected to one Na^+ ion by a single H_2O molecule. The anionic $(Cu_4I_6)^{2-}$ cluster is formed by CuI_3 (Cu^+ coordinated by three I^-) units connected *via* edges and nodes. The BCNCI crystals exhibit a broadband yellowish emission with a peak centered at around 548 nm, upon light irradiation at 365 nm (UV) and 450 nm (blue). The two components in the broadband yellow emission, caused by the MLCT/HLCT and CC transitions, are more pronounced and clearly revealed at low temperatures (cryogenic range). The yellow crystals have superior broadband emission with high PLQYs reaching 99.1% and 82% for 365 nm and 450 nm photoluminescence excitation. These organic copper(I) iodide clusters are ideally suited for solid-state lighting applications due to their exceptional moisture stability and broadband yellow emission encompassing the visible region under UV/blue light excitation.

Data availability

Data will be available on request.

Conflicts of interest

There are no conflicts to declare.

Acknowledgements

SAK acknowledges the support from Hoffmann Institute of Advanced Materials, Shenzhen Polytechnic University, P. R. China. This research used the Advanced Light Source (ALS), which is a DOE Office of Science User Facility under contract No. DE-AC02-05CH11231. The authors also extend their sincere appreciation to the Researchers Supporting Project (RSP2025R29) at King Saud University, Riyadh, Saudi Arabia.

References

1 J. Luo, X. Wang, S. Li, J. Liu, Y. Guo, G. Niu, L. Yao, Y. Fu, L. Gao and Q. Dong, Efficient and stable emission of warm-white light from lead-free halide double perovskites, *Nature*, 2018, **563**(7732), 541–545.
2 E. R. Dohner, E. T. Hoke and H. I. Karunadasa, Self-assembly of broadband white-light emitters, *J. Am. Chem. Soc.*, 2014, **136**(5), 1718–1721.
3 K. T. Bicanic, X. Li, R. P. Sabatini, N. Hossain, C.-F. Wang, F. Fan, H. Liang, S. Hoogland and E. H. Sargent, Design of phosphor white light systems for high-power applications, *ACS Photonics*, 2016, **3**(12), 2243–2248.
4 A. C. Berends, M. A. van de Haar and M. R. Krames, YAG:Ce^{3+} phosphor: from micron-sized workhorse for general lighting to a bright future on the nanoscale, *Chem. Rev.*, 2020, **120**(24), 13461–13479.
5 C. He, H. Ji, Z. Huang, T. Wang, X. Zhang, Y. Liu, M. Fang, X. Wu, J. Zhang and X. Min, Red-shifted emission in $Y_3MgSiAl_3O_{12}$: Ce^{3+} garnet phosphor for blue light-pumped white light-emitting diodes, *J. Phys. Chem. C*, 2018, **122**(27), 15659–15665.
6 S. A. Khan, N. Z. Khan, M. Sohail, J. Ahmed, N. Alhokbany, S. M. Alshehri, X. Xu, J. Zhu and S. Agathopoulos, Modern aspects of strategies for developing single-phase broadly tunable white light-emitting phosphors, *J. Mater. Chem. C*, 2021, **9**(38), 13041–13071.
7 W. Ye, C. Zhao, X. Shen, C. Ma, Z. Deng, Y. Li, Y. Wang, C. Zuo, Z. Wen and Y. Li, High quantum yield $Gd_{4.67}Si_3O_{13}$: Eu^{3+} red-emitting phosphor for tunable white light-emitting devices driven by UV or blue LED, *ACS Appl. Electron. Mater.*, 2021, **3**(3), 1403–1412.
8 S. Ferrara, J. P. Fernandéz-Blázquez, J. P. Fuenzalida Werner and R. D. Costa, Homopolymeric Protein Phosphors: Overpassing the Stability Frontier of Deep-Red Bio-Hybrid Light-Emitting Diodes, *Adv. Funct. Mater.*, 2023, 2300350.
9 P. Dang, G. Li, X. Yun, Q. Zhang, D. Liu, H. Lian, M. Shang and J. Lin, Thermally stable and highly efficient red-emitting Eu^{3+}-doped $Cs_3GdGe_3O_9$ phosphors for WLEDs: non-concentration quenching and negative thermal expansion, *Light: Sci. Appl.*, 2021, **10**(1), 29.
10 A. Kojima, K. Teshima, Y. Shirai and T. Miyasaka, Organometal halide perovskites as visible-light sensitizers for photovoltaic cells, *J. Am. Chem. Soc.*, 2009, **131**(17), 6050–6051.
11 Y. Xu, X. Hu, H. Tang, Q. Hu, S. Wang, T. Chen, X. Zhang, W. Jiang, L. Wang and W. Jiang, Highly efficient silica coated perovskite nanocrystals with the assistance of ionic liquids for warm white LEDs, *Nanoscale*, 2023, **15**(2), 631–643.
12 J. Chen, J. Wang, X. Xu, J. Li, J. Song, S. Lan, S. Liu, B. Cai, B. Han and J. T. Precht, Efficient and bright white light-emitting diodes based on single-layer heterophase halide perovskites, *Nat. Photonics*, 2021, **15**(3), 238–244.
13 H. Lin, C. Zhou, Y. Tian, T. Siegrist and B. Ma, Low-dimensional organometal halide perovskites, *ACS Energy Lett.*, 2017, **3**(1), 54–62.
14 Y. Wang, S. Guo, H. Luo, C. Zhou, H. Lin, X. Ma, Q. Hu, M.-H. Du, B. Ma and W. Yang, Reaching 90% photoluminescence

quantum yield in one-dimensional metal halide $C_4N_2H_{14}PbBr_4$ by pressure-suppressed nonradiative loss, *J. Am. Chem. Soc.*, 2020, **142**(37), 16001–16006.

15 Z. Liu, W. Qiu, X. Peng, G. Sun, X. Liu, D. Liu, Z. Li, F. He, C. Shen and Q. Gu, Perovskite Light-Emitting Diodes with EQE Exceeding 28% through a Synergetic Dual-Additive Strategy for Defect Passivation and Nanostructure Regulation, *Adv. Mater.*, 2021, **33**(43), 2103268.

16 J. Jiang, Z. Chu, Z. Yin, J. Li, Y. Yang, J. Chen, J. Wu, J. You and X. Zhang, Red perovskite light-emitting diodes with efficiency exceeding 25% realized by cospacer cations, *Adv. Mater.*, 2022, **34**(36), 2204460.

17 Y. Shen, Y. Q. Li, K. Zhang, L. J. Zhang, F. M. Xie, L. Chen, X. Y. Cai, Y. Lu, H. Ren and X. Gao, Multifunctional Crystal Regulation Enables Efficient and Stable Sky-Blue Perovskite Light-Emitting Diodes, *Adv. Funct. Mater.*, 2022, **32**(41), 2206574.

18 Y. Yu, Y. Tang, B. Wang, K. Zhang, J. X. Tang and Y. Q. Li, Red Perovskite Light-Emitting Diodes: Recent Advances and Perspectives, *Laser Photonics Rev.*, 2022, 2200608.

19 M. D. Smith and H. Karunadasa, White-light emission from layered halide perovskites, *Acc. Chem. Res.*, 2018, **51**(3), 619–627.

20 E. R. Dohner, A. Jaffe, L. R. Bradshaw and H. I. Karunadasa, Intrinsic white-light emission from layered hybrid perovskites, *J. Am. Chem. Soc.*, 2014, **136**(38), 13154–13157.

21 T. Jun, K. Sim, S. Iimura, M. Sasase, H. Kamioka, J. Kim and H. Hosono, Lead-free highly efficient blue-emitting $Cs_3Cu_2I_5$ with 0D electronic structure, *Adv. Mater.*, 2018, **30**(43), 1804547.

22 B. Yang, L. Yin, G. Niu, J. H. Yuan, K. H. Xue, Z. Tan, X. S. Miao, M. Niu, X. Du and H. Song, Lead-Free Halide Rb_2CuBr_3 as Sensitive X-Ray Scintillator, *Adv. Mater.*, 2019, **31**(44), 1904711.

23 C. Zhou, H. Lin, M. Worku, J. Neu, Y. Zhou, Y. Tian, S. Lee, P. Djurovich, T. Siegrist and B. Ma, Blue emitting single crystalline assembly of metal halide clusters, *J. Am. Chem. Soc.*, 2018, **140**(41), 13181–13184.

24 L. Zhou, J. F. Liao, Z. G. Huang, J. H. Wei, X. D. Wang, W. G. Li, H. Y. Chen, D. B. Kuang and C. Y. Su, A highly red-emissive lead-free indium-based perovskite single crystal for sensitive water detection, *Angew. Chem., Int. Ed.*, 2019, **131**(16), 5331–5335.

25 C. Pareja-Rivera, J. A. Morán-Muñoz, A. P. Gómora-Figueroa, V. Jancik, B. Vargas, J. Rodríguez-Hernández and D. Solis-Ibarra, Optimizing Broadband Emission in 2D Halide Perovskites, *Chem. Mater.*, 2022, **34**(21), 9344–9349.

26 G. Zhang, D. Wang, B. Lou, C. G. Ma, A. Meijerink and Y. Wang, Efficient Broadband Near-Infrared Emission from Lead-Free Halide Double Perovskite Single Crystal, *Angew. Chem., Int. Ed.*, 2022, **61**(33), e202207454.

27 M. Zhang, L. Zhao, J. Xie, Q. Zhang, X. Wang, N. Yaqoob, Z. Yin, P. Kaghazchi, S. Zhang and H. Li, Molecular engineering towards efficientwhite-light-emitting perovskite, *Nat. Commun.*, 2021, **12**(1), 1–7.

28 I. López-Fernández, D. Valli, C. Y. Wang, S. Samanta, T. Okamoto, Y. T. Huang, K. Sun, Y. Liu, V. S. Chirvony and A. Patra, Lead-Free Halide Perovskite Materials and Optoelectronic Devices: Progress and Prospective, *Adv. Funct. Mater.*, 2024, **34**(6), 2307896.

29 G. Zhang, D. Wang, B. Lou, C. G. Ma, A. Meijerink and Y. Wang, Efficient broadband near-infrared emission from lead-free halide double perovskite single crystal, *Angew. Chem., Int. Ed.*, 2022, **61**(33), e202207454.

30 S. Fang, H. Li, Y. Xie, H. Li, Y. Wang and Y. Shi, Zero-Dimensional Organic–Inorganic Hybrid Copper-Based Halides with Highly Efficient Orange–Red Emission, *Small*, 2021, **17**(42), 2103831.

31 S. A. Khan, C. Li, A. Jalil, X. Xin, M. Rauf, J. Ahmed, M. M. Khan, B. Dong, J. Zhu and S. Agathopoulos, Development of structure and tuning ability of the luminescence of lead-free halide perovskite nanocrystals (NCs), *Chem. Eng. J.*, 2021, **420**, 127603.

32 X.-K. Liu, W. Xu, S. Bai, Y. Jin, J. Wang, R. H. Friend and F. Gao, Metal halide perovskites for light-emitting diodes, *Nat. Mater.*, 2021, **20**(1), 10–21.

33 S. A. Khan, N. Z. Khan, M. Sohail, M. Runowski, X. Xu and S. Agathopoulos, Recent Developments of Lead-Free Halide-Perovskite Nanocrystals: Synthesis Strategies, Stability, Challenges, and Potential in Optoelectronic Applications, *Mater. Today Phys.*, 2023, 101079.

34 X. Hei, W. Liu, K. Zhu, S. J. Teat, S. Jensen, M. Li, D. M. O'Carroll, K. Wei, K. Tan and M. Cotlet, Blending ionic and coordinate bonds in hybrid semiconductor materials: a general approach toward robust and solution-processable covalent/coordinate network structures, *J. Am. Chem. Soc.*, 2020, **142**(9), 4242–4253.

35 K. Zhu, Z. Cheng, S. Rangan, M. Cotlet, J. Du, L. Kasaei, S. J. Teat, W. Liu, Y. Chen and L. C. Feldman, A New Type of Hybrid Copper Iodide as Nontoxic and Ultrastable LED Emissive Layer Material, *ACS Energy Lett.*, 2021, **6**(7), 2565–2574.

36 Y. Fang, K. Zhu, S. J. Teat, O. G. Reid, X. Hei, K. Zhu, X. Fang, M. Li, C. A. Sojdak and M. Cotlet, Robust and Highly Conductive Water-Stable Copper Iodide-Based Hybrid Single Crystals, *Chem. Mater.*, 2022, **34**(22), 10040–10049.

37 W. Ki, X. Hei, H. T. Yi, W. Liu, S. J. Teat, M. Li, Y. Fang, V. Podzorov, E. Garfunkel and J. Li, Two-Dimensional Copper Iodide-Based Inorganic–Organic Hybrid Semiconductors: Synthesis, Structures, and Optical and Transport Properties, *Chem. Mater.*, 2021, **33**(13), 5317–5325.

38 H. Li, Y. Lv, Z. Zhou, H. Tong, W. Liu and G. Ouyang, Coordinated Anionic Inorganic Module—An Efficient Approach Towards Highly Efficient Blue-Emitting Copper Halide Ionic Hybrid Structures, *Angew. Chem., Int. Ed.*, 2022, **61**(8), e202115225.

39 B. Su, J. Jin, Y. Peng, M. S. Molokeev, X. Yang and Z. Xia, Zero-Dimensional Organic Copper(I) Iodide Hybrid with High Anti-Water Stability for Blue-Light-Excitable Solid-State Lighting, *Adv. Opt. Mater.*, 2022, 2102619.

40 T. Jun, K. Sim, S. Iimura, M. Sasase, H. Kamioka, J. Kim and H. Hosono, Lead-free highly efficient blue-emitting

$Cs_3Cu_2I_5$ with 0D electronic structure, *Adv. Mater.*, 2018, **30**(43), 1804547.

41 L. Lian, M. Zheng, P. Zhang, Z. Zheng, K. Du, W. Lei, J. Gao, G. Niu, D. Zhang and T. Zhai, Photophysics in $Cs_3Cu_2X_5$ (X = Cl, Br, or I): highly luminescent self-trapped excitons from local structure symmetrization, *Chem. Mater.*, 2020, **32**(8), 3462–3468.

42 T. D. Creason, T. M. McWhorter, Z. Bell, M.-H. Du and B. Saparov, K_2CuX_3 (X = Cl, Br): all-inorganic lead-free blue emitters with near-unity photoluminescence quantum yield, *Chem. Mater.*, 2020, **32**(14), 6197–6205.

43 X. Hei and J. Li, All-in-one: a new approach toward robust and solution-processable copper halide hybrid semiconductors by integrating covalent, coordinate and ionic bonds in their structures, *Chem. Sci.*, 2021, **12**(11), 3805–3817.

44 A. V. Artem'ev, M. P. Davydova, X. Hei, M. I. Rakhmanova, D. G. Samsonenko, I. Y. Bagryanskaya, K. A. Brylev, V. P. Fedin, J.-S. Chen and M. Cotlet, Family of robust and strongly luminescent CuI-Based hybrid networks made of ionic and dative bonds, *Chem. Mater.*, 2020, **32**(24), 10708–10718.

45 X. Hei, S. J. Teat, W. Liu and J. Li, Eco-friendly, solution-processable and efficient low-energy lighting phosphors: copper halide based hybrid semiconductors $Cu_4X_6(L)_2$ (X = Br, I) composed of covalent, ionic and coordinate bonds, *J. Mater. Chem. C*, 2020, **8**(47), 16790–16797.

46 X. Meng, S. Ji, Q. Wang, X. Wang, T. Bai, R. Zhang, B. Yang, Y. Li, Z. Shao and J. Jiang, Organic–Inorganic Hybrid Cuprous-Based Metal Halides for Warm White Light-Emitting Diodes. Advanced, *Science*, 2022, **9**(31), 2203596.

47 Y. Tong, A. Najar, L. Wang, L. Liu, M. Du, J. Yang, J. Li, K. Wang and S. Liu, Wide-Bandgap Organic–Inorganic Lead Halide Perovskite Solar Cells, *Adv. Sci.*, 2022, **9**(14), 2105085.

48 H. Mo, Y.-C. Yin, J.-D. Luo, J.-T. Yang, F. Li, D.-M. Huang, H. Zhang, B. Ye, T. Tian and H.-B. Yao, Lead-Free Solid-State Organic–Inorganic Halide Perovskite Electrolyte for Lithium-Ion Conduction, *ACS Appl. Mater. Int.*, 2022, **14**(15), 17479–17485.

49 H. Wang, Z. Chen, F. Tian, G. Zheng, H. Wang, T. Zhang, J. Qin, X. Gao, P. A. van Aken and L. Zhang, Impacts of the Lattice Strain on Perovskite Light-Emitting Diodes, *Adv. Energy Mater.*, 2022, 2202185.

50 S. Li, J. Xu, Z. Li, Z. Zeng, W. Li, M. Cui, C. Qin and Y. Du, One-dimensional lead-free halide with near-unity greenish-yellow light emission, *Chem. Mater.*, 2020, **32**(15), 6525–6531.

51 J. Huang, B. Su, E. Song, M. S. Molokeev and Z. Xia, Ultra-broad-band-excitable Cu(I)-based organometallic halide with near-unity emission for light-emitting diode applications, *Chem. Mater.*, 2021, **33**(12), 4382–4389.

52 T. Zheng, M. Runowski, I. R. Martín, K. Soler-Carracedo, L. Peng, M. Skwierczyńska, M. Sójka, J. Barzowska, S. Mahlik and H. Hemmerich, Mechanoluminescence and photoluminescence heterojunction for superior multimode sensing platform of friction, force, pressure, and temperature in fibers and 3D-printed polymers, *Adv. Mater.*, 2023, **35**(40), 2304140.

53 M. Runowski, P. Woźny, I. R. Martín, K. Soler-Carracedo, T. Zheng, H. Hemmerich, F. Rivera-López, J. Moszczyński, P. Kulpiński and S. Feldmann, Multimodal Optically Nonlinear Nanoparticles Exhibiting Simultaneous Higher Harmonics Generation and Upconversion Luminescence for Anticounterfeiting and 8-bit Optical Coding, *Adv. Funct. Mater.*, 2024, **34**(1), 2307791.

54 X. Qiu, T. Zheng, M. Runowski, P. Woźny, I. R. Martín, K. Soler-Carracedo, C. E. Piñero, S. Lebedkin, O. Fuhr and S. Bräse, Constructing [2.2] Paracyclophane-Based Ultrasensitive Optical Fluorescent-Phosphorescent Thermometer with Cucurbit [8] uril Supramolecular Assembly, *Adv. Funct. Mater.*, 2024, 2313517.

55 L. Mao, P. Guo, M. Kepenekian, I. Hadar, C. Katan, J. Even, R. D. Schaller, C. C. Stoumpos and M. G. Kanatzidis, Structural diversity in white-light-emitting hybrid lead bromide perovskites, *J. Am. Chem. Soc.*, 2018, **140**(40), 13078–13088.

56 G. Wu, C. Zhou, W. Ming, D. Han, S. Chen, D. Yang, T. Besara, J. Neu, T. Siegrist and M.-H. Du, A one-dimensional organic lead chloride hybrid with excitation-dependent broadband emissions, *ACS Energy Lett.*, 2018, **3**(6), 1443–1449.

57 G. F. Kresse, Jürgen Efficient iterative schemes for ab initio total-energy calculations using a plane-wave basis set, *Phys. Rev. B: Condens. Matter Mater. Phys.*, 1996, **54**(16), 11169.

58 P. E. Blöchl, Projector augmented-wave method, *Phys. Rev. B: Condens. Matter Mater. Phys.*, 1994, **50**(24), 17953.

59 G. Kresse, Joubert, Daniel From ultrasoft pseudopotentials to the projector augmented-wave method, *Phys. Rev. B: Condens. Matter Mater. Phys.*, 1999, **59**(3), 1758.

60 J. P. B. Perdew, Kieron Ernzerhof, Matthias Generalized gradient approximation made simple, *Phys. Rev. Lett.*, 1996, **77**(18), 3865.

61 S. Grimme, J. Antony, S. Ehrlich and H. Krieg, A consistent and accurate ab initio parametrization of density functional dispersion correction (DFT-D) for the 94 elements H-Pu. The, *J. Chem. Phys.*, 2010, **132**(15), 154104.

62 R. Peng, M. Li and D. Li, Copper(I) halides: A versatile family in coordination chemistry and crystal engineering, *Coord. Chem. Rev.*, 2010, **254**(1–2), 1–18.

63 S. A. Khan, N. Z. Khan, Z. Hao, W. W. Ji, H. Abadikhah, L. Hao, X. Xu and S. Agathopoulos, Influence of substitution of Al-O for Si-N on improvement of photoluminescence properties and thermal stability of $Ba_2Si_5N_8$: Eu^{2+} red emitting phosphors, *J. Alloys Compd.*, 2018, **730**, 249–254.

64 S. A. Khan, A. Jalil, Q. U. Khan, R. M. Irfan, I. Mehmood, K. Khan, M. Kiani, B. Dong, N. Z. Khan and J.-L. Yu, New physical insight into crystal structure, luminescence and optical properties of YPO4: Dy^{3+}\$Eu^{3+}$\$Tb^{3+}$ single-phase white-light-emitting phosphors, *J. Alloys Compd.*, 2020, **817**, 152687.

65 S. A. Khan, H. Zhong, W. Ji, L.-Y. Hao, H. Abadikhah, X. Xu, N. Z. Khan and S. Agathopoulos, Single-phase white light-emitting $Ca_xBa_{(9-x)}Lu_2Si_6O_{24}$: Eu^{2+}/Mn^{2+} phosphors, *ACS Omega*, 2017, **2**(9), 6270–6277.

66 N. Z. Khan, S. A. Khan, A. Jalil, F. Wang, I. Mehmood, M. T. Abbas, L. Ali, M. Sohail, X. Xu and S. Agathopoulos, Structural development and luminescent enhancement of

$CaAlSiN_3$: Eu^{2+} phosphor via replacing Al^{3+} by Ga^{3+}, *J. Alloys Compd.*, 2022, **897**, 162485.

67 S. A. Khan, N. Z. Khan, N. Muhammad, F. Lin, M. Runowski, J. Ahmed, S. Agathopoulos and J. Li, Highly efficient and tunable broadband UV excitable $Ba_9Lu_2Si_6O_{24}$: Eu^{2+}, Mn^{2+} single-phase white-light-emitting phosphors, *J. Alloys Compd.*, 2023, **938**, 168650.

68 W. Liu, Y. Fang, G. Z. Wei, S. J. Teat, K. Xiong, Z. Hu, W. P. Lustig and J. Li, A family of highly efficient CuI-based lighting phosphors prepared by a systematic, bottom-up synthetic approach, *J. Am. Chem. Soc.*, 2015, **137**(29), 9400–9408.

69 X. Liu, Y. Li, T. Liang, W. Liu and J. Fan, One-Center and Two-Center Self-Trapped Excitons in Zero-Dimensional Hybrid Copper Halides: Tricolor Luminescence with High Quantum Yields, *J. Phys. Chem. Lett.*, 2022, **13**(5), 1373–1381.

70 M. Yao, G. Xu, K. Tang, M. Zhang, B. Zhang and J. Zhu, Synthesis, crystal growth, electronic structures and optical properties of wide bandgap semiconductor $(CH_3NH_3)_2HgI_4$, *J. Solid State Chem.*, 2023, 124116.

71 Y. Fang, W. Liu, S. J. Teat, G. Dey, Z. Shen, L. An, D. Yu, L. Wang, D. M. O'Carroll and J. Li, A Systematic Approach to Achieving High Performance Hybrid Lighting Phosphors with Excellent Thermal-and Photostability, *Adv. Funct. Mater.*, 2017, **27**(3), 1603444.

72 P. C. Ford and A. Vogler, Photochemical and photophysical properties of tetranuclear and hexanuclear clusters of metals with d10 and s2 electronic configurations, *Acc. Chem. Res.*, 1993, **26**(4), 220–226.

73 Y. Fang, C. A. Sojdak, G. Dey, S. J. Teat, M. Li, M. Cotlet, K. Zhu, W. Liu, L. Wang and D. M. ÓCarroll, Highly efficient and very robust blue-excitable yellow phosphors built on multiple-stranded one-dimensional inorganic–organic hybrid chains, *Chem. Sci.*, 2019, **10**(20), 5363–5372.

74 R. Czerwieniec, M. J. Leitl, H. H. Homeier and H. Yersin, Cu(I) complexes–Thermally activated delayed fluorescence. Photophysical approach and material design, *Coord. Chem. Rev.*, 2016, **325**, 2–28.

75 M. J. Leitl, V. A. Krylova, P. I. Djurovich, M. E. Thompson and H. Yersin, Phosphorescence versus thermally activated delayed fluorescence. Controlling singlet–triplet splitting in brightly emitting and sublimable Cu(I) compounds, *J. Am. Chem. Soc.*, 2014, **136**(45), 16032–16038.

76 B. Huitorel, H. El Moll, R. Utrera-Melero, M. Cordier, A. Fargues, A. Garcia, F. Massuyeau, C. Martineau-Corcos, F. Fayon and A. Rakhmatullin, Evaluation of ligands effect on the photophysical properties of copper iodide clusters, *Inorg. Chem.*, 2018, **57**(8), 4328–4339.

77 K. R. Kyle, C. K. Ryu, P. C. Ford and J. A. DiBenedetto, Photophysical studies in solution of the tetranuclear copper(I) clusters $Cu_4I_4L_4$ (L = pyridine or substituted pyridine), *J. Am. Chem. Soc.*, 1991, **113**(8), 2954–2965.

78 Q. Benito, X. F. Le Goff, G. Nocton, A. Fargues, A. Garcia, A. Berhault, S. Kahlal, J.-Y. Saillard, C. Martineau and J. Trébosc, Geometry flexibility of copper iodide clusters: Variability in luminescence thermochromism, *Inorg. Chem.*, 2015, **54**(9), 4483–4494.

79 C. K. Ryu, K. R. Kyle and P. C. Ford, Photoluminescence properties of the copper (I) chloride clusters $Cu_4Cl_4L_4$ (L = pyridine, substituted pyridine, or saturated amine), *Inorg. Chem.*, 1991, **30**(21), 3982–3986.

80 C. K. Ryu, M. Vitale and P. C. Ford, Photoluminescence properties of the structurally analogous tetranuclear copper(I) clusters $Cu_4X_4(dpmp)_4$ (X = I, Br, Cl; dpmp = 2-(diphenylmethyl) pyridine), *Inorg. Chem.*, 1993, **32**(6), 869–874.

81 G. Song, M. Li, S. Zhang, N. Wang, P. Gong, Z. Xia and Z. Lin, Enhancing photoluminescence quantum yield in 0D metal halides by introducing water molecules, *Adv. Funct. Mater.*, 2020, **30**(32), 2002468.

82 B. Su, J. Jin, Y. Peng, M. S. Molokeev, X. Yang and Z. Xia, Zero-Dimensional Organic Copper(I) Iodide Hybrid with High Anti-Water Stability for Blue-Light-Excitable Solid-State Lighting, *Adv. Opt. Mater.*, 2022, **10**(12), 2102619.

83 M. Chen, C. Ye, C. Dai, R. Qi, H. Fu, C. Luo, H. Peng and H. Lin, Highly Luminescent Copper(I) Halide Phosphors Encapsulated in Fumed Silica for Anti-Counterfeiting and Color-Converting Applications, *Adv. Opt. Mater.*, 2022, **10**(13), 2200278.

84 A. Mensah, J.-J. Shao, J.-L. Ni, G.-J. Li, F.-M. Wang and L.-Z. Chen, Recent progress in luminescent Cu(I) halide complexes: A mini-review, *Front. Chem.*, 2022, **9**, 816363.

85 S. A. Khan, Z. Hao, W. W. Ji, N. Z. Khan, H. Abadikhah, L. Hao, X. Xu, S. Agathopoulos and Q. Bao, Crystal-site engineering for developing tunable green light emitting $Ba_9Lu_2Si_6O_{24}$: Eu^{2+} phosphors for efficient white LEDs, *J. Alloys Compd.*, 2018, **767**, 374–381.

86 S. A. Khan, A. Jalil, Q. U. Khan, R. M. Irfan, I. Mehmood, K. Khan, M. Kiani, B. Dong, N. Z. Khan and J.-L. Yu, New physical insight into crystal structure, luminescence and optical properties of YPO4: Dy^{3+}\$Eu^{3+}$\$Tb^{3+}$ single-phase white-light-emitting phosphors, *J. Alloys Compd.*, 2020, **817**, 152687.

87 M. Xie and J. Tian, Operational stability issues and challenges in metal halide perovskite light-emitting diodes, *J. Phys. Chem. Lett.*, 2022, **13**(8), 1962–1971.

88 W. Xiang, S. F. Liu and W. Tress, A review on the stability of inorganic metal halide perovskites: challenges and opportunities for stable solar cells, *Energy Environ. Sci.*, 2021, **14**(4), 2090–2113.

89 Z. Zhu, Q. Sun, Z. Zhang, J. Dai, G. Xing, S. Li, X. Huang and W. Huang, Metal halide perovskites: stability and sensing-ability, *J. Mater. Chem. C*, 2018, **6**(38), 10121–10137.

90 Q. Tu, D. Kim, M. Shyikh and M. G. Kanatzidis, Mechanics-coupled stability of metal-halide perovskites, *Matter*, 2021, **4**(9), 2765–2809.

91 H. Cho, Y. H. Kim, C. Wolf, H. D. Lee and T. W. Lee, Improving the stability of metal halide perovskite materials and light-emitting diodes, *Adv. Mater.*, 2018, **30**(42), 1704587.

92 L. Zhu, H. Cao, C. Xue, H. Zhang, M. Qin, J. Wang, K. Wen, Z. Fu, T. Jiang and L. Xu, Unveiling the additive-assisted oriented growth of perovskite crystallite for high

performance light-emitting diodes, *Nat. Commun.*, 2021, **12**(1), 5081.

93 Q. Zhang, S. Liu, M. He, W. Zheng, Q. Wan, M. Liu, X. Liao, W. Zhan, C. Yuan and J. Liu, Stable Lead-Free Tin Halide Perovskite with Operational Stability > 1200 h by Suppressing Tin(II) Oxidation, *Angew. Chem., Int. Ed.*, 2022, **61**(30), e202205463.

94 Y. Cai, W. Li, D. Tian, S. Shi, X. Chen, P. Gao and R. J. Xie, Organic Sulfonium-Stabilized High-Efficiency Cesium or Methylammonium Lead Bromide Perovskite Nanocrystals, *Angew. Chem.*, 2022, **134**(37), e202209880.

95 B. Guo, R. Lai, S. Jiang, L. Zhou, Z. Ren, Y. Lian, P. Li, X. Cao, S. Xing and Y. Wang, Ultrastable near-infrared perovskite light-emitting diodes, *Nat. Photonics*, 2022, **16**(9), 637–643.